Physical Inputs for Simulations of Gravitational Wave Emissions from Compact Stars within the Einstein Telescope Detection Range

Caden Phillips

A report submitted in partial fulfilment of the requirements for the
PHYS309: Physics Internship module at the
University of Liverpool

Work conducted at the Instytut Fizyki Jądrowej, Krakow, Poland

Academic Supervisor: Dr. Uta Klein
Host Supervisor: Dr. David Alvarez Castillo

September 19, 2025

Contents

Abstract

The cores of neutron stars (NS) may contain exotic states of matter such as deconfined quarks. Recent detections of gravitational waves (GW) have opened the door to this new physics. This project aimed to utilise a set of hybrid Equations of State (EoS), characterised by a phase transition from hadronic to quark matter within these cores, to model the macroscopic properties of neutron stars. A Fisher Information Matrix framework was implemented to forecast parameter estimation errors and a Python-based Tolman-Oppenheimer-Volkoff (TOV) solver was developed to compute mass-radius (M-R) and tidal deformability-mass (Λ-M) relations from 62 hybrid EoS files, each modelling 400 NS. Analysis of these stars revealed that stable configurations have maximum masses ranging from 2.0 to 2.4 $M_\odot$ and radii from 11 to 13 km, depending on the EoS. For a typical 1.4 $M_\odot$ star, the tidal deformability, Λ, ranges from 100 to 800. These results were then compared with observational constraints from GW170817. Further analysis of these stars identified unique signatures within the first-order phase transition such as the potential for stable twin star configurations. This work demonstrates the ability of GW analysis to better understand the fundamental properties of neutron stars and provides crucial inputs for future detectors like the Einstein Telescope.

Introduction

The Origins of Gravitational Waves Astronomy

On September 14, 2015, the first gravitational wave (GW) was detected [1]. The signal, GW150914, originated from the merger of two black holes and was captured by the Laser Interferometer Gravitational-Wave Observatory (LIGO) [1, 2]. This detection confirmed a major prediction of Einstein's general theory of relativity published a century prior, the existence of gravitational waves [7] and marked the birth of a new field of astronomy, providing a new method to study these phenomena. Although GW150914 was instrumental, the observation on August 17, 2017, GW170817, truly revolutionised the field [3]. The signal was generated by the inspiral and merger of two neutron stars, generating a spectrum-wide electromagnetic signal [4]. This event generated both gravitational and electromagnetic information that can be combined to create a complete picture of the astrophysical event. This binary neutron star (BNS) merger contained more than just information about spacetime dynamics; it carried imprints of the internal structure of the neutron stars themselves, offering an unprecedented opportunity to probe the nature of matter under the most extreme conditions found in the cosmos [5, 8].

The Equation of State of Neutron Stars Once massive stars undergo a supernova explosion, it may leave behind a neutron star from its core [16]. They are amongst the densest objects within the universe with masses of up to 2.5 $M_\odot$ with a radius of 10 to 15 km [16, 17]. The physics governing the matter within these objects are described by the Equation of State (EoS), which relates the pressure of the matter to its energy density [16, 18]. The EoS is fundamental to the physical structure of the star; however, it is a poorly understood aspect of nuclear physics. Contrastingly, the outer layers of neutron stars are relatively well understood – the outer crust consists of a lattice of neutron-rich nuclei immersed in a highly degenerate electron gas, while in the inner crust, above the "neutron drip" density, there is a lattice of nuclei permeated by a superfluid of neutrons that flow through the lattice; the intense densities lead the core to remain a mystery [19]. At these intense densities within the inner core, the constituent neutrons may dissolve into their constituent quarks and gluons, creating a state of matter known as deconfined quark matter. [16]. An EoS can be modelled to incorporate this change from hadronic to quark matter, this is known as a "hybrid" EoS [16, 18]. Many theoretical models exist for both hadronic and quark matter, this results in a large range of possibilities for hybrid EoS candidates [16, 18]. Determining which of these models is a prime objective of modern astrophysics, as it would reveal fundamental properties of the strong nuclear force [17, 18].

Tidal Deformability in Neutron Stars Gravitational waves from BNS mergers, such as GW170817, provide information that can be used to constrain the EoS [3, 5, 8]. During the end of the system's inspiral, the massive gravitational field of both stars causes a tidal bulge in its companion star [8, 10]. The resistance to this deformation is determined by its internal structure and is defined as the tidal deformability, Λ [8, 10]. If the star has a "stiff" EoS (pressure increases rapidly with density) it will be less compact and less resistant to the deformation, resulting in a larger Λ. Whereas, if the EoS is "soft" it will be more compact and more resistant to the deformation, causing a smaller Λ [10]. This interaction affects the orbiting phase of the inspiral, leaving a measurable imprint on the gravitational waveform [8]. In order to determine how well a detector can measure parameters such as Λ, one can use statistical forecast tools such as the Fisher matrix [15]. This provides us a powerful method to estimate the statistical errors on physical parameters within the gravitational wave signal. By calculating these forecasted errors, one can assess the feasibility of distinguishing between different EoS models with current and future detectors [11].

Project Aims This project was designed to use the known principles of neutron stars to explore the viability of different sets of hybrid EoS models [15, 16]. Specifically, the objectives were:

- Implementation and analysis of a Fisher Matrix Framework for GW estimation, including tidal deformability as a fifth parameter [15].
- Development of a TOV solver in Python capable of taking a hybrid EoS as an input and calculating the macroscopic properties of a neutron star [12, 14].
- Analysis of large EoS model datasets to generate a catalogue of M-R and Λ-M relations [16, 18].
- Identify unique properties such as strong first-order phase transitions, such as the twin stars [16, 18].

- Compare theoretical predictions with observational constraints to filter the EoS dataset and remove anything which is not physically possible [3, 5].

1 Methodology

The project was completed based on a plan that progressed from statistical forecasting to data production and analysis. The core of this plan was the development of a comprehensive Python-based analysis pipeline.

Fisher matrix The initial part of the project focused on calculating statistical errors using the Fisher matrix (F_{ij}) formalism, a standard approach for forecasting parameter-estimation precision in gravitational-wave astronomy [15]. As noted by Vallisneri (2008), Fisher analyses provide a useful first-order approximation but often underestimate true uncertainties at low signal-to-noise ratios, a caveat considered when interpreting our results. For a signal h dependent on a set of parameters θ, the matrix is defined by the inner product:

$$F_{ij} = \left\langle \frac{\partial h}{\partial \theta_i}, \frac{\partial h}{\partial \theta_j} \right\rangle \tag{1}$$

Where the inverse of this matrix, F^{-1}, is the covariance matrix, whose diagonal elements provide the variance (σ_i^2) and thus the statistical error for each parameter [15]. Here, $\langle a, b \rangle$ denotes the noise-weighted inner product, $\theta = \{t_c, \phi_c, \ln \mathcal{M}, \ln \eta\}$ are the parameters of the waveform (t_c: coalescence time, ϕ_c: coalescence phase, $\mathcal{M}$: chirp mass, η: symmetric mass ratio), and σ_i^2 is the variance of parameter i. To improve the physical accuracy, we replaced the analytic power spectral density (PSD) approximation with a digitised, frequency-dependent noise curve (ET-D design sensitivity), ensuring realistic noise weighting in the inner-product integral used for SNR and Fisher calculations.

Incorporating Tidal Deformability Once the Fisher matrix has been created, one can extend it to include the effects of tidal deformability, a key observable for constraining the EoS. This effect is parameterised by the mass-weighted average tidal deformability, $\tilde{\Lambda}$, defined as [8, 10]:

$$\tilde{\Lambda} = \frac{16}{13} \cdot \frac{(m_1 + 12m_2)m_1^4\Lambda_1 + (m_2 + 12m_1)m_2^4\Lambda_2}{(m_1 + m_2)^5} \tag{2}$$

Here, m_1 and m_2 are the component masses of the binary system, Λ_1 and Λ_2 are the tidal deformabilities of each individual star, and $\tilde{\Lambda}$ is the mass-weighted tidal deformability of the binary. This tidal deformability is calculated using the dimensionless second Love number, k_2, of each star and their compactness ($C = GM/(Rc^2)$) [8, 10]:

$$\Lambda = \frac{2}{3} k_2 C^{-5} \tag{3}$$

Where the Love number, k_2, is a complex function of the star's internal structure which is calculated by solving a differential equation alongside the TOV equations. The tidal effect introduces a phase shift in the gravitational waveform, given at the lowest order by :

$$\Psi_{\text{tidal}} = -\frac{39}{2} \tilde{\Lambda} v^{10} \tag{4}$$

The waveform derivatives with respect to all parameters, including $\tilde{\Lambda}$, were computed numerically using finite differences with step sizes chosen to ensure convergence ($< 1\%$ relative change when halved). However, it is important to note that the Fisher matrix often underestimates true uncertainties [15]). This extended the Fisher matrix to 5×5 dimensions, including correlations between $\tilde{\Lambda}$ and the other four parameters. This new matrix accounts for the degeneracies from the tidal parameter and the four initial parameters ($\{t_c, \phi_c, \ln \mathcal{M}, \ln \eta\}$).

Constructing the Hybrid EoS This project focused on the analysis of different hybrid EoS files. These hybrid EoS were constructed by stitching hadronic and quark matter branches together using a Maxwell construction, following detailed instructions provided [22]. To determine which point these EoS files are stitched, one first plots a graph of Pressure P against Chemical Potential μ. At the point where the hadronic and quark branches overlap, this is where the first-order phase transition occurs and as such, the region below this point is hadronic and after is quark matter [16]. The dataset was constructed to explore the specific quark matter model by varying the effective gluon mass (M_g), with the files organised into four categories: 500, 600, 700, and 800 MeV. Here, P denotes pressure, μ the chemical potential, and M_g the effective gluon mass, which was varied between 500–800 MeV to generate different quark matter models. Figure 1 shows the combined pressure–chemical potential curves for all 62 hybrid EoS files that exhibit a valid phase transition, with each line corresponding to a different quark matter model.

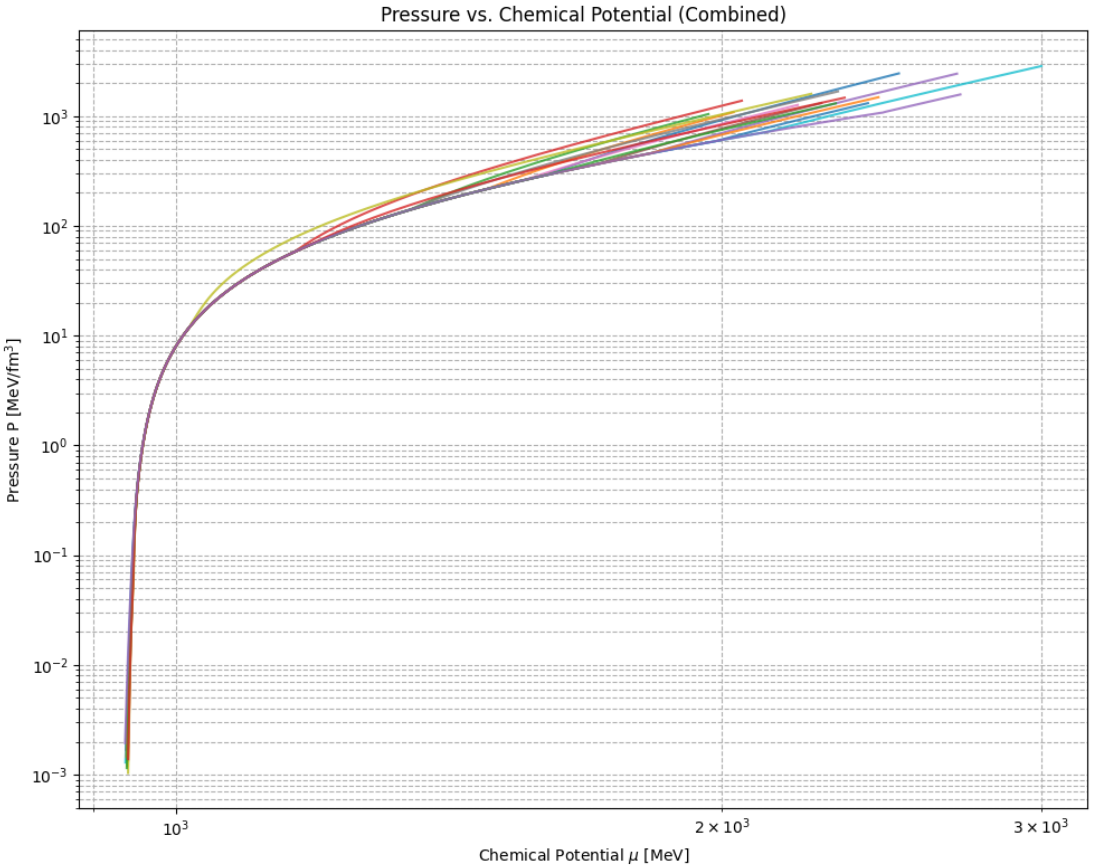

Figure 1: Combined pressure–chemical potential curves for all 62 hybrid EoS files that exhibit a valid phase transition. Each line corresponds to a different quark matter model.

Tolman-Oppenheimer-Volkoff (TOV) Solver To model neutron-star structure, a FORTRAN-based TOV solver [12, 14] was re-implemented in Python and integrated with the analysis pipeline. The solver was benchmarked against published SLy and APR mass–radius and tidal deformability curves, showing agreement better than 1%, giving confidence in the accuracy of the results. This program numerically solves the TOV equations:

$$\frac{dM(r)}{dr} = 4\pi r^2 \epsilon(r) \tag{5}$$

$$\frac{dp(r)}{dr} = -\frac{[\epsilon(r) + p(r)][M(r) + 4\pi r^3 p(r)]}{r(r - 2M(r))} \tag{6}$$

In these equations, $M(r)$ is the enclosed gravitational mass, $\epsilon(r)$ the energy density, and $p(r)$ the pressure at radius r. This solver was combined with the code to calculate the Love number, k_2, and the tidal deformability, Λ, for each stable star modelled [8, 10], and used to analyse each of the 62 hybrid EoS files that demonstrate a first-order phase transition. Figure 2 presents the pressure–energy density curves for the same 62 hybrid EoS models, again with each line representing a different quark matter model. This view is used to check the thermodynamic stability and ensure a consistent phase transition construction. Applying the TOV solver to each of the 62 hybrid EoS files highlights how sensitive the properties of neutron stars are to changes in the quark matter parameters. Even minor changes to the initial parameters of the EoS produce noticeably different outcomes for the neutron star. This demonstrates the power of the TOV solver as a diagnostic tool: small changes on the microscopic level cascade into significant differences at the macroscopic level.

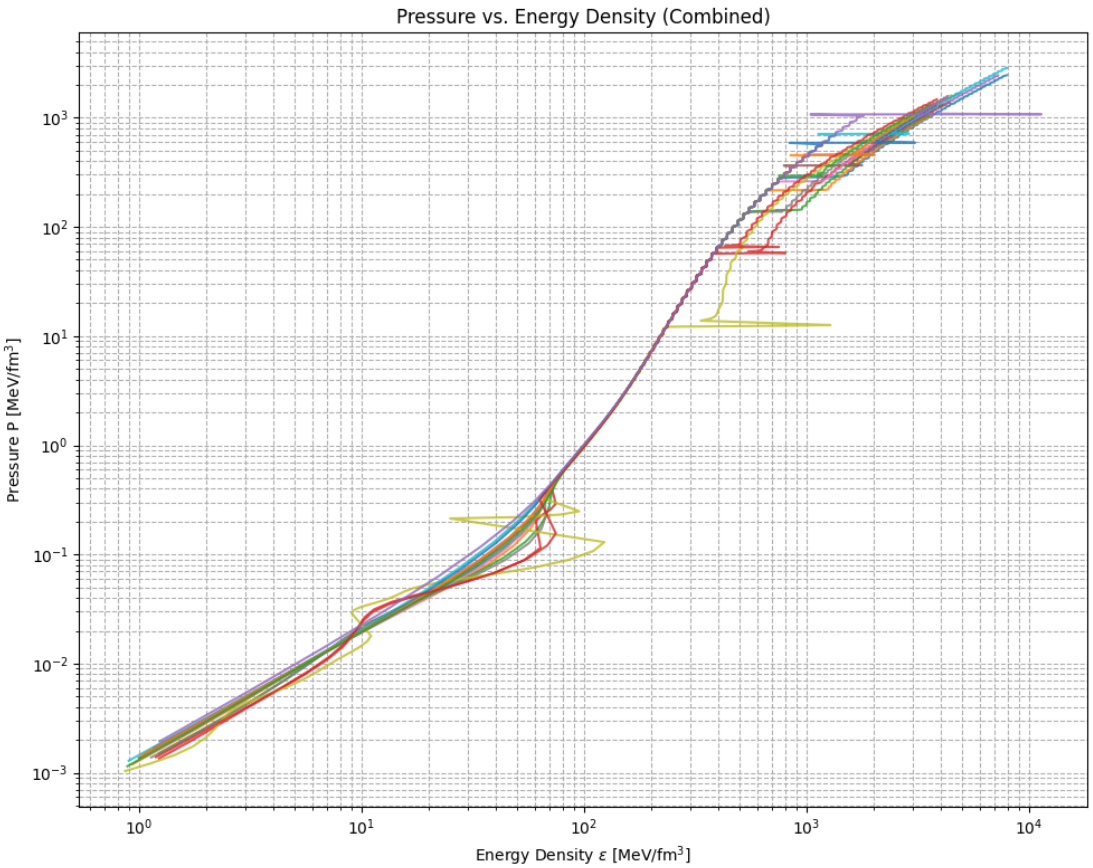

Figure 2: Pressure–energy density curves for all 62 hybrid EoS files. Each line represents a different quark matter model.

(A full list of symbols is provided in Appendix A.)

2 Results and Discussion

Fisher Matrix Analysis The 5-parameter Fisher analysis shows that including the tidal deformability, $\tilde{\Lambda}$, as a free parameter introduces correlations with $\mathcal{M}_c$ and η, which broaden their measurement uncertainties across all Post-Newtonian (PN) orders. Here, $\mathcal{M}_c = \frac{(m_1 m_2)^{3/5}}{(m_1+m_2)^{1/5}}$ is the chirp mass, and $\eta = \frac{m_1 m_2}{(m_1+m_2)^2}$ is the symmetric mass ratio. This occurs due to the degeneracies between the parameters [15]; information in the waveform that could be used to measure the chirp mass with more accuracy is now being used to measure the tidal deformability. This concession in gaining information about tidal deformability at the expense of accuracy of the other parameters is a fundamental aspect of gravitational wave data analysis. Table 1 and Table 2 forecast the errors for the 4-parameter and 5-parameter models, clearly indicating this increase in uncertainty following the addition of Λ. Although the Fisher matrix is a widely used tool in determining the statistical uncertainties in measuring the properties of GW, its tendency to underestimate these uncertainties at low SNR means that Bayesian parameter estimation would be preferable in future studies [23].

Table 1: 4-Parameter Fisher Results [15]

System	PN Order	SNR	Δt_c (ms)	$\Delta\phi_c$ (rad)	$\Delta\mathcal{M}/\mathcal{M}$ (%)	$\Delta\eta/\eta$ (%)	Max Amplitude
NS-NS	1PN	10	0.237	0.532	0.567	0.005	1.72E-23
NS-NS	1.5PN	10	0.341	1.303	1.269	0.002	1.72E-23
NS-NS	2PN	10	0.348	1.193	1.869	0.003	1.72E-23
NS-NS	2.5PN	10	0.217	0.264	0.608	0.004	1.72E-23
NS-NS	3PN	10	0.247	0.220	0.565	0.004	1.72E-23
NS-NS	3.5PN	10	0.228	0.232	0.580	0.004	1.72E-23
NS-BH	1PN	10	0.165	0.330	0.680	0.005	1.74E-23
NS-BH	1.5PN	10	0.217	0.607	0.408	0.002	1.74E-23
NS-BH	2PN	10	0.210	0.512	0.511	0.002	1.74E-23
NS-BH	2.5PN	10	0.340	0.674	0.657	0.004	1.74E-23
NS-BH	3PN	10	0.168	0.608	0.550	0.004	1.74E-23
NS-BH	3.5PN	10	0.374	0.608	0.641	0.004	1.74E-23
BH-BH	1PN	10	0.132	0.195	1.189	0.028	1.95E-23
BH-BH	1.5PN	10	0.191	0.400	0.768	0.015	1.95E-23
BH-BH	2PN	10	0.172	0.284	1.026	0.014	1.95E-23
BH-BH	2.5PN	10	0.476	0.481	1.216	0.029	1.95E-23
BH-BH	3PN	10	0.105	0.518	0.816	0.024	1.95E-23
BH-BH	3.5PN	10	0.325	0.532	0.969	0.026	1.95E-23

Table 2: 5-Parameter Fisher Results including the 1-σ uncertainty in $\tilde{\Lambda}$ (computed from the inverse Fisher matrix) [15].

System	PN Order	SNR	Δt_c (ms)	$\Delta\phi_c$ (rad)	$\Delta\mathcal{M}/\mathcal{M}$ (%)	$\Delta\eta/\eta$ (%)	$\Delta\tilde{\Lambda}$	Max Amplitude
NS-NS	1PN	10	0.372739	0.873949	1.104682	0.010740	4229.181	7.033e-24
NS-NS	1.5PN	10	0.536468	2.009115	1.990073	0.002189	4606.837	7.033e-24
NS-NS	2PN	10	0.534669	1.769608	2.805773	0.003396	4607.323	7.033e-24
NS-NS	2.5PN	10	0.325957	0.340797	1.091519	0.008213	4305.175	7.033e-24
NS-NS	3PN	10	0.387720	0.271637	1.010196	0.007855	4373.203	7.033e-24
NS-NS	3.5PN	10	0.347545	0.288370	1.037480	0.007981	4343.478	7.033e-24
NS-BH	1PN	10	0.557905	0.878247	1.818255	0.014065	361.628	7.080e-24
NS-BH	1.5PN	10	0.768013	1.682581	1.070414	0.006751	416.239	7.080e-24
NS-BH	2PN	10	0.734693	1.402707	1.320425	0.006502	408.645	7.080e-24
NS-BH	2.5PN	10	0.751213	1.593021	1.548158	0.011427	289.108	7.080e-24
NS-BH	3PN	10	0.334892	1.458863	1.344233	0.010552	324.063	7.080e-24
NS-BH	3.5PN	10	0.825331	1.440339	1.514665	0.011284	292.525	7.080e-24
BH-BH	1PN	10	0.371338	0.370024	2.023698	0.054087	116.555	7.663e-24
BH-BH	1.5PN	10	0.635801	0.990517	1.753675	0.039810	146.934	7.663e-24
BH-BH	2PN	10	0.495951	0.595410	1.933128	0.031844	128.813	7.663e-24
BH-BH	2.5PN	10	0.783298	0.794849	1.974822	0.056870	101.207	7.663e-24
BH-BH	3PN	10	0.235302	1.082004	1.765672	0.059643	124.875	7.663e-24
BH-BH	3.5PN	10	0.582837	1.008818	1.858597	0.059093	111.396	7.663e-24

Note: $\Delta\tilde{\Lambda}$ is the 1-σ Fisher matrix uncertainty on the mass-weighted tidal deformability, not its physical value.

These results show that for all binary types (NS-NS, NS-BH, BH-BH), the uncertainties increase across all PN orders when tidal deformability is added. Interestingly, the Neutron Star-Black Hole (NS-BH) binary systems exhibit the largest increase in error, indicating that tidal effects introduce significant new degeneracies in these asymmetric systems.

Mass-Radius Relations The primary function of the TOV solver is to produce a mass–radius (M–R) relation for each EoS (see Figure 3 for an example EoS). Figure 4 illustrates the large spread of M–R curves caused by variations in the quark matter parameters such as gluon mass. According to observations of massive pulsars, all viable models must be able to sustain a maximum mass of at least 2 $M_\odot$. This dataset predicts a maximum mass for stable hybrid stars from 2.0 to 2.4 $M_\odot$, with radii in the stable branch between 11 and 13 km. These values are consistent with observations of massive pulsars, such as PSR J0348+0432, which set the empirical lower bound for viable EoS models, and with theoretical studies by Lattimer & Prakash [16, 17]. Figure 4 compares the mass–radius relations for all 62 hybrid EoS models, with solid lines

indicating stable branches and dashed lines showing the unstable branches. Figure 3 operates as a representative of the M-R curve for the stable hybrid star. It shows the full sequence of equilibrium stellar configurations, from very low mass stars up to the onset of instability. Beginning at the bottom-left of Figure 3, the curve has four distinct segments. Initially, it shows a rising mass and radius with strong internal pressure, a plateau where the EoS reaches its maximum stellar radius as internal pressure balances with gravitational compression [16, 18], the turnover as the radius begins to decrease as mass increases due to the gravitational strength becoming so intense that the star becomes more compact to counteract this, finally, the unstable branch where equilibrium solutions exist mathematically but are unstable to perturbations.

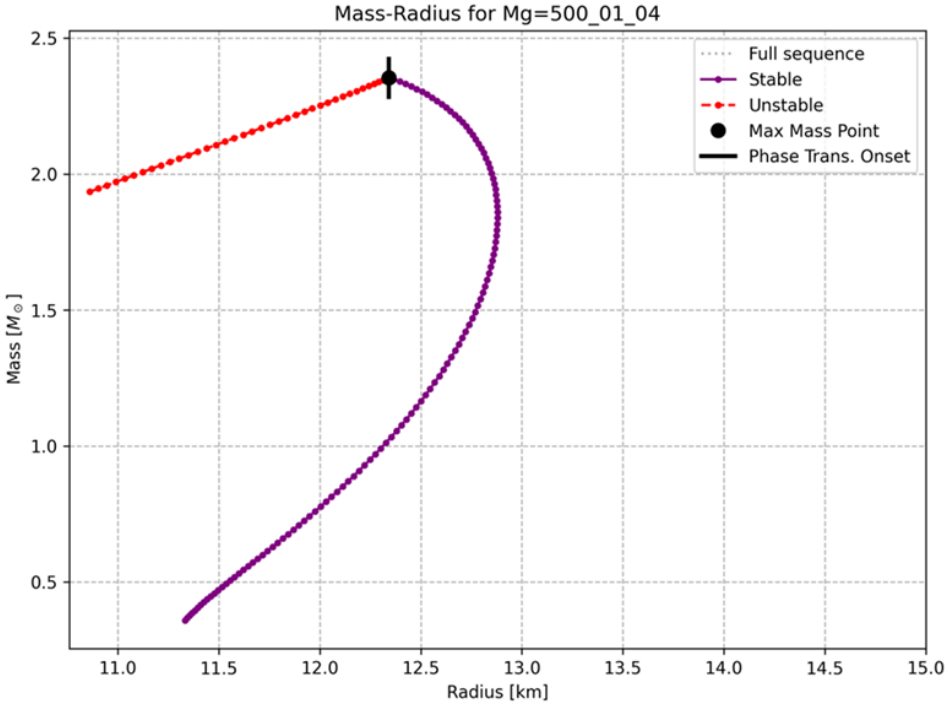

Figure 3: Mass–radius relation from EoS file Mg=500_01_04

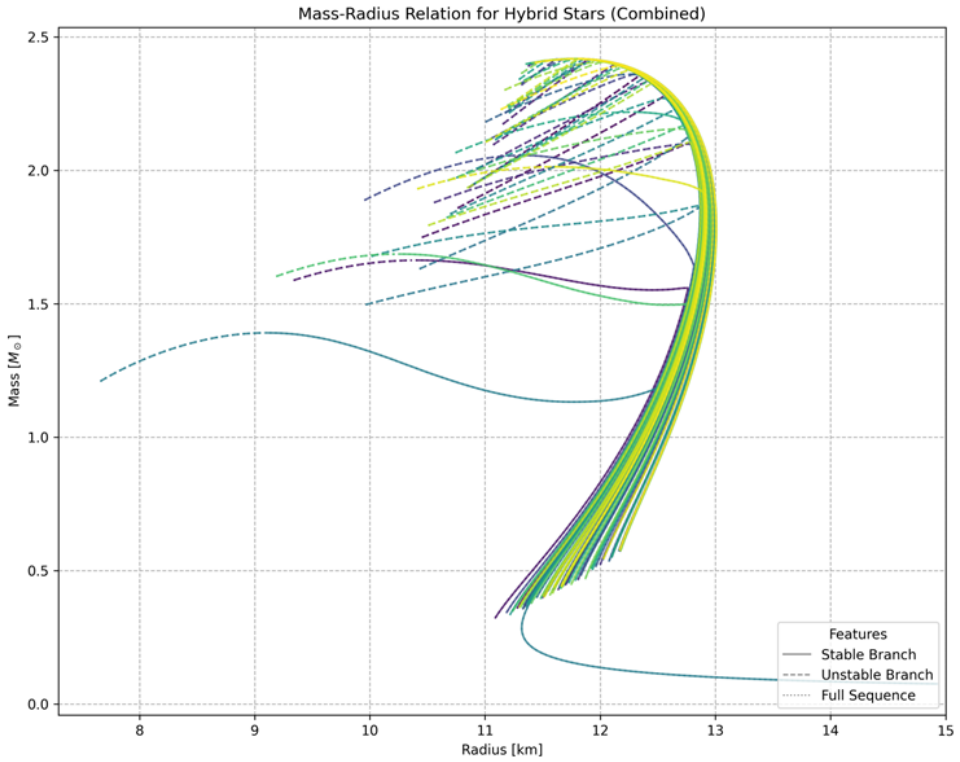

Figure 4: Mass–radius relations for all 62 hybrid EoS models. Solid lines represent stable branches, and dashed lines represent unstable branches.

Possible Twin Stars One key finding of this project was that some very soft EoS models can demonstrate a strong

first-order phase transition that can produce a second branch of stable stars. This leads to a phenomenon called twin stars where two stable stars can exist with the same mass but different radii [16, 18]. One of these stars is larger and purely hadronic, whereas the twin is a smaller and more compact hybrid star. While this phenomenon is still without any observational proof, an observational discovery of such a pair would provide incontrovertible evidence for a strong phase transition inside neutron stars. Figure 5 provides an example of a hybrid EoS that predicts such a twin-star configuration, clearly showing two distinct stable branches. As shown in Figure 5, for a mass of about 1.2 $M_\odot$ two solutions exist — a hadronic star with a radius of ≈ 12.5 km and a more compact hybrid twin with ≈ 7.8 km radius. Figure 5 also shows that some hybrid EoS models predict that if a neutron star has a very low mass, around 0.2 $M_\odot$, their central densities will be low enough to reduce the gravitational strength to a low enough value to allow the star to expand to very large radii without becoming unstable. It should be emphasised that no neutron star with a mass below 1.174 $M_\odot$ has been observed. The lightest precisely measured case is the secondary in the asymmetric double NS system PSR J0453+1559, with a mass of $1.174 \pm 0.004\, M_\odot$ [21], consistent with the observational summary of [17]. Theoretical studies of minimum NS mass also suggest a lower bound of similar order [20].

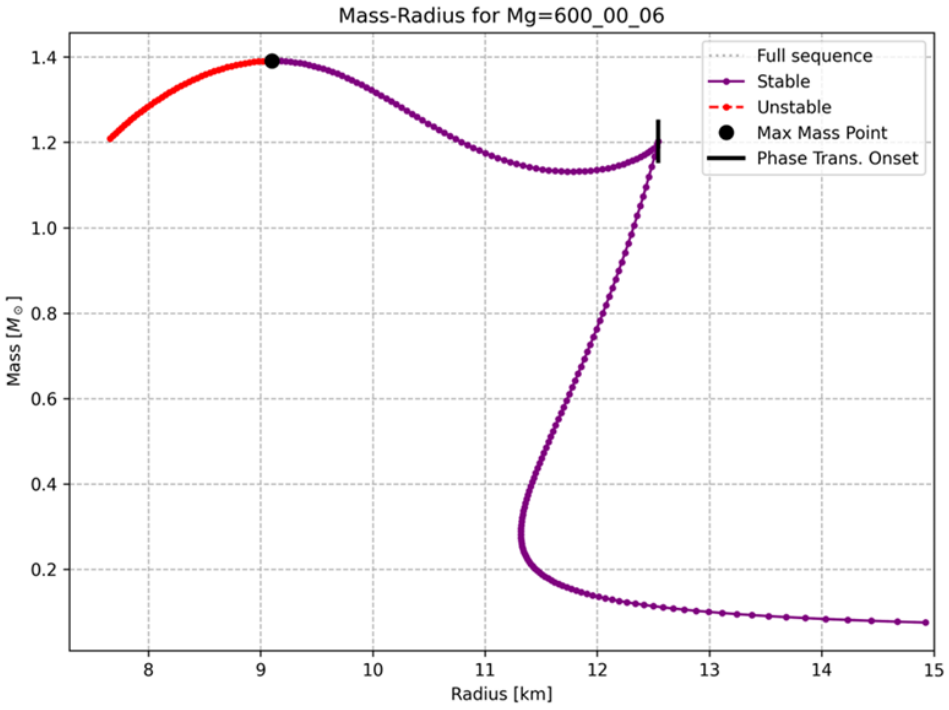

Figure 5: Mass–radius relation for EoS file Mg=600_00_06, showing two distinct stable branches corresponding to hadronic and hybrid-star solutions.

Tidal Deformability By analysing the tidal deformability one can obtain a more sensitive probe into the star's internal structure, as shown in Figure 6. For a typical 1.4 $M_\odot$ star, the predicted value of Λ varies significantly, from approximately 100 to 800, spanning the 90% credible intervals inferred from GW170817 [3, 5]. This highlights the strong discriminating power of tidal measurements: further improvements in Λ constraints could immediately rule out a large fraction of current hybrid EoS candidates. This demonstrates the wide range of predictions from different EoS models. Phase transitions leave a dramatic signature that can be observed in the Λ-M plot in features such as the dramatic drop and a "hook" feature at the large masses. Both of these provide strong evidence for the presence of a quark core. Figure 6 illustrates the tidal deformability–mass relations for all 62 hybrid EoS models, with stable branches shown as solid curves and unstable branches as dashed.

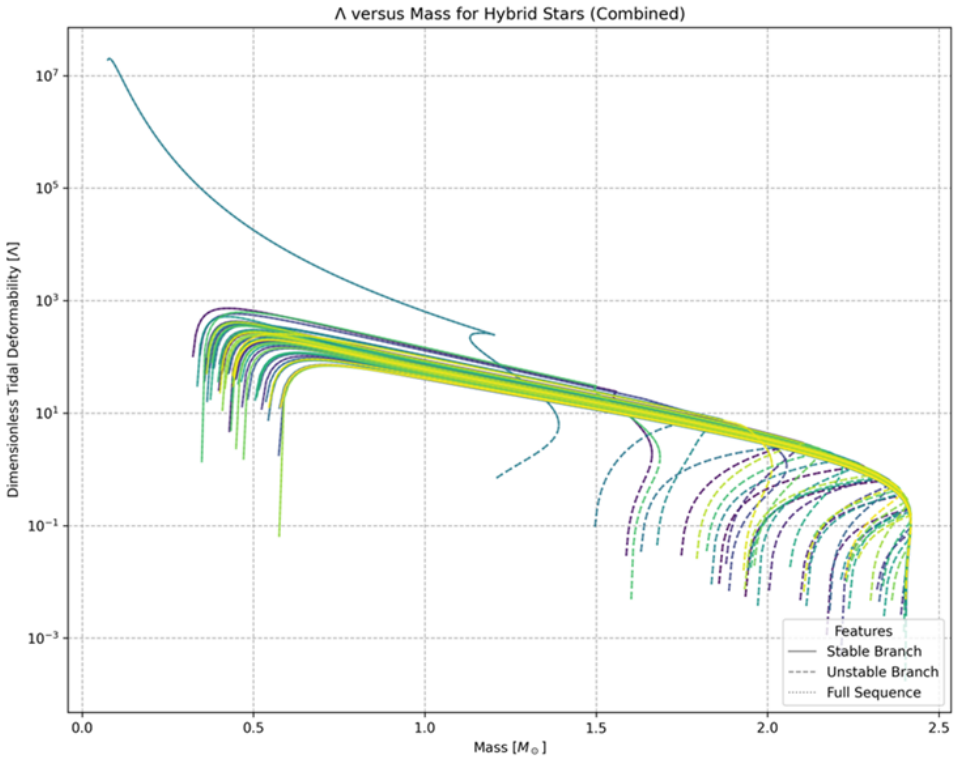

Figure 6: Tidal deformability–mass relations for all 62 hybrid EoS models. Stable branches are solid; unstable branches are dashed.

Constraints and Limitations The final step of the analysis was to constrain these predictions with observational data. By overlaying the 50% and 90% confidence regions from the GW170817 event [3, 5] onto the generated Λ-M plots, one can directly test each EoS, as seen in Figure 7. Should the model not pass through these observational contours, such models can be ruled out as inconsistent with observations. This process operates as a powerful way to filter these EoS files and significantly reduce the number of possible candidates. Figure 7 shows this comparison explicitly, overlaying the model-predicted Λ–M curves with the 50% and 90% credible intervals inferred from GW170817. As seen in Figure 7, all the theoretical predictions fall outside the 50% and 90% confidence regions. Therefore, the EoS used in this project are strongly disfavoured and can be ruled out. The primary limitations of this project are found within the TOV solver. The TOV equations make several assumptions, including perfect spherical symmetry, zero temperature, and no rotation [12, 14]. While these are standard approximations in neutron-star modelling, they neglect potentially significant effects such as rotational flattening, thermal pressure contributions, and magnetic fields. More advanced models like RNS [13] or LORENE [9] include these effects and could be used for future extensions of this work. To study neutron stars in further detail, Einstein's field equations must be used, such as in the RNS model [13] or the LORENE model [9]. One other limitation to consider is the compactness limit. In this project, the Buchdahl Limit ($0 < C < 4/9$) was used to confine the range of possible neutron stars [6]. This limit states that for any static, spherically symmetric perfect-fluid star, the compactness must satisfy $C < 4/9$. However, this limit assumes a perfect-fluid star. Real neutron stars lie well below $C = 4/9$, so we use the Buchdahl limit only as a conservative upper bound and exclude models approaching it as unphysical [18].

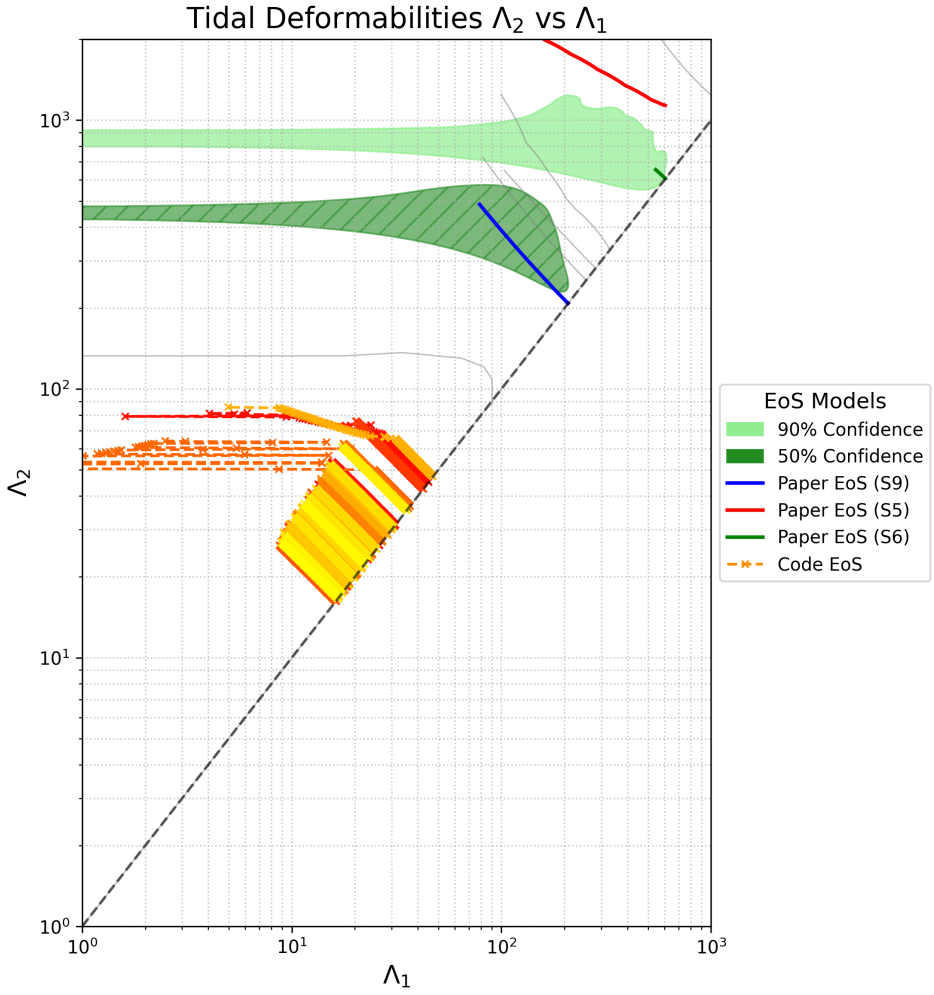

Figure 7: Comparison of model-predicted tidal deformability–mass relations with the 50% and 90% confidence intervals inferred from GW170817.

3 Conclusion and Outlook

Conclusion This project progressed in two stages — first, assessing statistical precision with an extended Fisher Information Matrix including tidal deformability, and second, exploring macroscopic properties of hybrid neutron stars using a Python-based Tolman–Oppenheimer–Volkoff (TOV) solver. The Fisher analysis quantified how adding tidal deformability as a fifth parameter increases measurement uncertainty but provides crucial sensitivity to the Equation of State (EoS) [15]. The TOV solver, benchmarked to within 1% against published results [12, 14], was applied to 62 hybrid EoS models to compute mass–radius and tidal deformability–mass relations. This analysis revealed maximum masses of 2.0–2.4 $M_\odot$, radii of 11–13 km, and in some cases, twin-star solutions — a distinctive signature of strong first-order phase transitions [16, 18]. Comparing these theoretical predictions with the observational data from GW170817, all tested models are found to be strongly disfavoured, demonstrating the power of gravitational-wave data to filter the EoS landscape [3, 5].

Outlook This work introduces a robust computational framework to systematically evaluate new EoS candidates, enabling the rejection of models that are inconsistent with observations. Future expansions of this project could incorporate rotational and thermal effects using tools such as `RNS` or `LORENE`, allowing more accurate and realistic modelling of neutron stars [13, 9]. Furthermore, replacing the Fisher-matrix approach with full Bayesian parameter estimation would produce more accurate statistical uncertainties, particularly at a lower SNR [23]. With the upcoming Einstein Telescope expected to detect hundreds of binary neutron star mergers per year, this methodology can be applied to a large statistical sample, potentially revealing signatures of hadron–quark phase transitions — including twin-star configurations — and offering direct evidence of quark matter in nature [11].

A List of Symbols and Acronyms

$\mathcal{M}_c$	Chirp mass, $\frac{(m_1 m_2)^{3/5}}{(m_1+m_2)^{1/5}}$
η	Symmetric mass ratio, $\frac{m_1 m_2}{(m_1+m_2)^2}$
m_1, m_2	Component masses of the binary
$M(r)$	Enclosed gravitational mass at radius r
$M_\odot$	Solar mass (mass of the Sun)
R	Stellar radius
$\epsilon(r)$	Energy density at radius r
$p(r)$	Pressure at radius r
P	Pressure (thermodynamic)
μ	Chemical potential
M_g	Effective gluon mass in quark matter model
k_2	Second (quadrupolar) Love number
C	Compactness, $GM/(Rc^2)$
Λ	Dimensionless tidal deformability
$\tilde{\Lambda}$	Mass-weighted tidal deformability
v	Post-Newtonian expansion parameter ($v = (\pi M f)^{1/3}$)
$\Psi_{\rm tidal}$	Tidal phase contribution to GW waveform
t_c	Coalescence time
ϕ_c	Coalescence phase
h	Gravitational waveform
$\langle a, b \rangle$	Noise-weighted inner product
σ_i^2	Variance of parameter i
Δ	Forecast uncertainty in a parameter (e.g. $\Delta\mathcal{M}/\mathcal{M}$)
GW	Gravitational Waves
NS	Neutron Star
BH	Black Hole
BNS	Binary Neutron Star
NS-BH	Neutron Star–Black Hole binary
M-R	Mass–Radius relation
EoS	Equation of State
Λ-M	Tidal Deformability-Mass relation
TOV	Tolman–Oppenheimer–Volkoff equations
PN	Post-Newtonian expansion order
PSD	Power Spectral Density
SNR	Signal-to-Noise Ratio

Acknowledgements

I would like to thank my host supervisor, Dr. David Alvarez Castillo, for his invaluable guidance and support throughout this project, and Dr. Syed Naqvi for his helpful discussions and advice. I am also grateful to my lab partner, Yaiza Cano, for her collaboration during the internship.

References

[1] B. P. Abbott et al. (LIGO Scientific Collaboration and Virgo Collaboration), Observation of Gravitational Waves from a Binary Black Hole Merger, Phys. Rev. Lett. 116, 061102 (2016).

[2] B. P. Abbott et al. (LIGO Scientific Collaboration and Virgo Collaboration), GW150914: The Advanced LIGO Detectors in the Era of First Discoveries, Phys. Rev. Lett. 116, 131103 (2016).

[3] B. P. Abbott et al. (LIGO Scientific Collaboration and Virgo Collaboration), GW170817: Observation of Gravitational Waves from a Binary Neutron Star Inspiral, Phys. Rev. Lett. 119, 161101 (2017).

[4] B. P. Abbott et al. (LIGO Scientific Collaboration and Virgo Collaboration), Multi-messenger Observations of a Binary Neutron Star Merger, Astrophys. J. Lett. 848, L12 (2017).

[5] B. P. Abbott et al. (LIGO Scientific Collaboration and Virgo Collaboration), Properties of the binary neutron star merger GW170817, Phys. Rev. X 9, 011001 (2019).

[6] H. A. Buchdahl, General Relativistic Fluid Spheres, Phys. Rev. 116, 1027 (1959).

[7] A. Einstein, Näherungsweise Integration der Feldgleichungen der Gravitation, Sitzungsber. K. Preuss. Akad. Wiss. Berlin 1916, 688 (1916).

[8] É. É. Flanagan and T. Hinderer, Constraining neutron-star tidal Love numbers with gravitational-wave detectors, Phys. Rev. D 77, 021502(R) (2008).

[9] E. Gourgoulhon, P. Grandclément, K. Taniguchi, J.-A. Marck, and S. Bonazzola, Quasiequilibrium sequences of synchronized and irrotational binary neutron stars in general relativity. I. Method and tests, Phys. Rev. D 63, 064029 (2001).

[10] T. Hinderer, Tidal Love Numbers of Neutron Stars, Astrophys. J. 677, 1216 (2008).

[11] M. Maggiore et al., Einstein Telescope: Science Case, Design Study and Feasibility Report, Report No. ET-0028A-20 (2020).

[12] J. R. Oppenheimer and G. M. Volkoff, On Massive Neutron Cores, Phys. Rev. 55, 374 (1939).

[13] N. Stergioulas and J. L. Friedman, Comparing models of rapidly rotating relativistic stars constructed by two different numerical methods, Astrophys. J. 444, 306 (1995).

[14] R. C. Tolman, Static Solutions of Einstein's Field Equations for Spheres of Fluid, Phys. Rev. 55, 364 (1939).

[15] M. Vallisneri, Use and abuse of the Fisher matrix in the assessment of gravitational-wave parameter-estimation prospects, Phys. Rev. D 77, 042001 (2008).

[16] J. M. Lattimer and M. Prakash, Neutron Star Structure and the Equation of State, Astrophys. J. 550, 426 (2001).

[17] F. Özel and P. Freire, Masses, Radii, and the Equation of State of Neutron Stars, Annu. Rev. Astron. Astrophys. 54, 401 (2016).

[18] J. M. Lattimer and M. Prakash, Neutron star observations: Prognosis for equation of state constraints, Phys. Rep. 442, 109 (2007).

[19] P. Haensel, "Neutron Star Crusts," in Physics of Neutron Star Interiors, edited by D. Blaschke, N.K. Glendenning, and A. Sedrakian, Lecture Notes in Physics, Vol. 578 (Springer-Verlag, Berlin, 2001), pp. 127–167.

[20] Y. Suwa, T. Yoshida, M. Shibata, H. Umeda, K. Takahashi, On the minimum mass of neutron stars, Mon. Not. R. Astron. Soc. 481, 3305–3312 (2018).

[21] J. G. Martinez, K. Stovall, P. C. C. Freire, et al., "Pulsar J0453+1559: A Double Neutron Star System with a Large Mass Asymmetry," Astrophys. J. 812, 143 (2015).

[22] D. Alvarez Castillo, instructions for constructing hybrid EoS and TOV solver usage (private communication, 2025).

[23] J. Veitch et al., Parameter estimation for compact binaries with ground-based gravitational-wave observations using the LALInference software library, Phys. Rev. D 91, 042003 (2015).